(2)

OFFICE OF NAVAL RESEARCH

CONTRACT NO. N00014-90-J-1281

R&T Code 4134011

TECHNICAL REPORT NO. 15

DESORPTION PRODUCT YIELDS FOLLOWING Cl_2 ADSORPTION ON Si(111)7X7: COVERAGE AND TEMPERATURE DEPENDENCE

P. Gupta, P.A. Coon, B.G. Koehler and S.M. George

In Press

in

Surface Sicence

Stanford University
Department of Chemistry
Stanford, California 94305

April 12, 1991

Unclassified
SECURITY CLASSIFICATION OF THIS PAGE

REPORT DOCUMENTATION PAGE

1a. REPORT SECURITY CLASSIFICATION Unclassified	1b. RESTRICTIVE MARKINGS
2a. SECURITY CLASSIFICATION AUTHORITY	3. DISTRIBUTION / AVAILABILITY OF REPORT Approved for public release distribution unlimited
2b. DECLASSIFICATION / DOWNGRADING SCHEDULE	
4. PERFORMING ORGANIZATION REPORT NUMBER(S) Technical Report # 15	5. MONITORING ORGANIZATION REPORT NUMBER(S)
6a. NAME OF PERFORMING ORGANIZATION Department of Chemistry Stanford University 6b. OFFICE SYMBOL (If applicable)	7a. NAME OF MONITORING ORGANIZATION Office of Naval Research
6c. ADDRESS (City, State, and ZIP Code) Stanford, California 94305	7b. ADDRESS (City, State, and ZIP Code) Chemistry Program 800 North Quincy St. Arlington, VA 22217
8a. NAME OF FUNDING / SPONSORING ORGANIZATION Office of Naval Research 8b. OFFICE SYMBOL (If applicable)	9. PROCUREMENT INSTRUMENT IDENTIFICATION NUMBER N00014-90-J-1281-P00001
8c. ADDRESS (City, State, and ZIP Code) Chemistry Program, 800 N. Quincy St. Arlington, VA 22217	10. SOURCE OF FUNDING NUMBERS PROGRAM ELEMENT NO / PROJECT NO / TASK NO / WORK UNIT ACCESSION NO

11. TITLE (Include Security Classification)
Desorption Product Yields Following Cl_2 Adsorption on Si(111)7x7: Coverage and Temperature Dependence.

12. PERSONAL AUTHOR(S)
P. Gupta, P.A. Coon, B.G. Koehler and S.M. George

13a. TYPE OF REPORT	13b. TIME COVERED	14. DATE OF REPORT (Year, Month, Day)	15. PAGE COUNT
Technical	FROM _____ TO _____		

16. SUPPLEMENTARY NOTATION

17. COSATI CODES			18. SUBJECT TERMS (Continue on reverse if necessary and identify by block number)
FIELD	GROUP	SUB-GROUP	

19. ABSTRACT (Continue on reverse if necessary and identify by block number) Desorption product yields obtained following Cl_2 adsorption on Si(111)7x7 were studied using temperature-programmed desorption (TPD) and laser-induced thermal desorption (LITD) techniques. At low chloride coverages of $\Theta/\Theta_S < 0.6$ where Θ_S is the saturation chloride coverage, TPD experiments monitored $SiCl_2$ as the only desorption product at approximately 950 K. At higher chloride coverages of $\Theta/\Theta_S > 0.6$, a small $SiCl_4$ TPD signal was also monitored at 950 K along with an additional $SiCl_2$ TPD feature at 690 K. LITD experiments detected $SiCl_2$ as the only desorption product in the LITD yield at low chloride coverages of $\Theta/\Theta_S < 0.6$. $SiCl_2$ and $SiCl_3$ LITD signals were both observed at higher chloride coverages of $\Theta/\Theta_S > 0.6$. In temperature-programmed LITD studies, the $SiCl_2$ LITD signals persisted until 950 K, whereas the $SiCl_3$ LITD signals were only observed until 700 K. The magnitude of the $SiCl_3$ LITD signal following saturation Cl_2 exposures also decreased as a function of adsorption temperature. The $SiCl_2$ desorption products were assigned to the recombinative desorption of $SiCl+Cl \rightarrow SiCl_2$. The $SiCl_3$ siganls were attributed to either the direct desorption of $SiCl_3$ surface species or the recombinative desorption of $SiCl_2+Cl \rightarrow SiCl_3$. Based on photoemission and scanning tunneling microscopy investigations, the $SiCl_2$ and $SiCl_3$ desorption yields were correlated with the existence of moni-, di- and trichloride species on the Si(111)7x7 surface. CONTINUED ON REVERSE

20. DISTRIBUTION / AVAILABILITY OF ABSTRACT	21. ABSTRACT SECURITY CLASSIFICATION
☒ UNCLASSIFIED/UNLIMITED ☐ SAME AS RPT ☐ DTIC USERS	Unclassified
22a. NAME OF RESPONSIBLE INDIVIDUAL Dr. David L. Nelson/Dr. Mark Ross	22b. TELEPHONE (Include Area Code) (202) 696-4410
	22c. OFFICE SYMBOL

DD FORM 1473, 84 MAR 83 APR edition may be used until exhausted. All other editions are obsolete.

SECURITY CLASSIFICATION OF THIS PAGE

19. Many sililarities were also observed between the chlorides and hydrides on the Si(111) 7x7 surface.

Submitted to Surface Science

Desorption Product Yields Following Cl_2 Adsorption on Si(111) 7x7: Coverage and Temperature Dependence

P. Gupta, P.A. Coon, B.G. Koehler and S.M. George

Department of Chemistry, Stanford University,
Stanford, California 94305

Abstract

Desorption product yields obtained following Cl_2 adsorption on Si(111) 7x7 were studied using temperature-programmed desorption (TPD) and laser-induced thermal desorption (LITD) techniques. At low chloride coverages of $\Theta/\Theta_s < 0.6$, where Θ_s is the saturation chloride coverage, TPD experiments monitored $SiCl_2$ as the only desorption product at approximately 950 K. At higher chloride coverages of $\Theta/\Theta_s > 0.6$, a small $SiCl_4$ TPD signal was also monitored at 950 K along with an additional $SiCl_2$ TPD feature at 690 K. LITD experiments detected $SiCl_2$ as the only desorption product in the LITD yield at low chloride coverages of $\Theta/\Theta_s < 0.6$. $SiCl_2$ and $SiCl_3$ LITD signals were both observed at higher chloride coverages of $\Theta/\Theta_s > 0.6$. In temperature-programmed LITD studies, the $SiCl_2$ LITD signals persisted until 950 K, whereas the $SiCl_3$ LITD signals were only observed until 700 K. The magnitude of the $SiCl_3$ LITD signal following saturation Cl_2 exposures also decreased as a function of adsorption temperature. The $SiCl_2$ desorption products were assigned to the recombinative desorption of $SiCl + Cl \rightarrow SiCl_2$. The $SiCl_3$ LITD signals were attributed to either the direct desorption of $SiCl_3$ surface species or the recombinative desorption of $SiCl_2 + Cl \rightarrow SiCl_3$. Based on photoemission and scanning tunneling microscopy investigations, the $SiCl_2$ and $SiCl_3$ desorption yields were correlated with the existence of mono-, di- and trichloride species on the Si(111) 7x7 surface. Many similarities were also observed between the chlorides and hydrides on the Si(111) 7x7 surface.

I. Introduction

Chlorine plays an essential role during the plasma etching of silicon surfaces (1-3). The interaction between chlorine and silicon is also important in the epitaxial growth of silicon during chemical vapor deposition with $SiCl_4 + H_2$ or $SiCl_2H_2$ (4-6). An understanding of the structure and stability of chlorine on silicon surfaces is essential for a complete description of the surface reaction steps that define plasma etching and epitaxial growth processes.

Previous work on chlorine adsorption on silicon surfaces has focused on the nature of the chloride species obtained after various stages of chlorine adsorption. X-ray photoemission spectroscopy (XPS) studies have monitored the silicon oxidation state after a saturation chlorine exposure on Si(111) 7x7 at 300 K (7,8). These XPS investigations measured oxidation states that were consistent with the bonding of one, two and three chlorine atoms to individual silicon surface atoms (7,8). The photoemission studies also demonstrated that monochloride species were present at low chlorine coverages and di- and trichloride species were formed at higher chlorine coverages (7). Only monochloride species were observed to remain on the Si(111) 7x7 surface after annealing to 673 K (7).

The XPS studies (7,8) are in agreement with numerous theoretical and experimental investigations of the structure and properties of chlorine on Si(111) surfaces (9-17). These studies have concluded that the stable covalent binding configuration for chlorine on Si(111) is the onefold atop site. Chlorine binding energies, bond lengths and chemisorption geometries on Si(111) have also been calculated and assigned (14-17).

Only a few studies have focused on the desorption products obtained from a Si(111) surface following chlorine exposure (18-20). Very early mass spectrometric studies investigated the desorption products following a saturation Cl_2 exposure on a Si(111) 7x7 surface at 300 K. These studies yielded Cl and $SiCl_x$ signals where x=1,2,3,4 (18). The presence of the silicon-chloride species was assigned to the cracking of $SiCl_4$ in the electron impact ionizer of the mass spectrometer (18).

Early modulated molecular beam investigations explored the interaction of Cl_2 with a

Si(111) surface at temperatures above 1000 K (19). These studies showed that $SiCl_2$ was the primary desorption product. A recent temperature-programmed desorption (TPD) study of chlorine on Si(100) 2x1 surface has also observed $SiCl_2$ desorption along with $SiCl_4$ desorption (20). $SiCl_4$ desorbed from a low temperature desorption state at 400 K, whereas $SiCl_4$ and $SiCl_2$ both desorbed from a high temperature desorption state at 900 K (20).

Scanning tunneling microscopy (STM) studies have also recently investigated chlorine on Si(111) 7x7 surfaces (21-23). These STM investigations have demonstrated that chlorine interacts with the adatom dangling bonds at low coverage (21). As the coverage increases, the chlorine penetrates the relatively open structure of the Si(111) 7x7 surface and inserts itself into the bonds between the adatom and the atoms in the underlying rest atom layer (21,22). Identification of $SiCl_2$ and $SiCl_3$ species at the higher chlorine coverages was determined by the registry of the adatom with respect to the underlying rest atom layer (22).

Although previous studies have confirmed the presence of monochlorides at low chloride coverages and di- and trichlorides at higher chloride coverages, the functional dependence of these chloride species on coverage and temperature has not been investigated. In this paper, the desorption product yields were examined during and after Cl_2 adsorption on Si(111) 7x7. Laser-induced thermal desorption (LITD) and temperature-programmed desorption (TPD) techniques were used to study the product yields versus chlorine coverage and surface temperature. LITD experiments also examined the nature of the silicon-chloride desorption species at different adsorption temperatures following saturation Cl_2 exposures.

II. Experimental

A. Vacuum Chamber and Crystal Preparation

The experimental apparatus has been described in detail previously (24,25). The ultrahigh vacuum (UHV) chamber was pumped by a 300 l/s ion pump and a titanium sublimation pump. These pumps maintained background pressures of approximately 4 X 10^{-10} Torr during the experiments. The chamber was equipped with an Extrel C-50 quadrupole mass spectrometer for LITD and TPD studies. For analysis of surface order and composition, the chamber also contained a low energy electron diffraction (LEED) spectrometer and a cylindrical mirror analyzer for Auger electron spectroscopy (AES).

The single-crystal Si(111) wafers were obtained from Siltec Silicon. These Si(111) wafers were p-type, boron-doped with a thickness of 380 μm and resistivity of $\rho = 1.2\ \Omega$-cm. In addition, the angle of inclination of the surface plane with respect to the Si(111) plane was either $\alpha = 0 \pm 0.25\ ^\circ$ or $\alpha = 4.0 \pm 0.5\ ^\circ$ toward the [110] direction. These two angles of inclinations yielded equivalent results. An angle of inclination of $\alpha = 4.0^\circ$ is typical for device-grade Si(111) wafers used in epitaxial growth processing.

The Si(111) wafers were cut into rectangular samples with dimensions of 1.1 cm X 1.0 cm. Individual silicon samples were mounted on a liquid-nitrogen cooled cryostat on a differentially-pumped rotary feedthrough (26). The sample mounting design employed two tantalum foil clamps that has been described in detail previously (25). Sample cooling was achieved by mounting each tantalum foil clamp to a copper support block that was electrically isolated from the cryostat.

A 4000 Å thick tantalum film was deposited on the back of the silicon crystal to facilitate the resistive heating of the silicon sample. The sample was heated and temperature regulated by passing a dc current from a programmable power supply through the sample and the tantalum film. The wafer was electrically isolated from the copper support block by a 0.035 inch sapphire sheet. The lowest surface temperature that was obtained was 105 K. A W5%Re/W26%Re thermocouple

was used to measure the temperature of the silicon crystal. The thermocouple was attached directly to the silicon crystal using the methods described previously (24,25).

The Si(111) surface was initially cleaned in vacuum by slowly annealing the sample to approximately 1350 K. AES peak-to-peak heights for carbon (KLL), oxygen (KLL), chlorine (LMM) and silicon (LVV) were compared after this annealing procedure. Annealing to 1350 K for a period of two to five minutes was then repeated until the C : Si, O : Si and Cl : Si AES ratios were less than 1×10^{-3}. Samples cleaned in this manner produced sharp 7x7 LEED patterns. The crystal was cleaned by annealing the silicon sample at 1350 K for two minutes following each Cl_2 exposure.

B. LITD and TPD Studies

Laser-induced thermal desorption (LITD) experiments utilized a TEM-00 Q-switched Ruby laser. The laser pulses had a temporal width (FWHM) of 80 - 100 ns and a Gaussian spatial profile. The pulses were focused onto the silicon sample using a 1.0 m lens. The focused laser beam had a Gaussian spatial profile with a width of 260 μm (FWHM). The laser pulse energy was approximately 3.5 mJ before entering the viewport of the UHV chamber.

The laser pulses were incident on the silicon chamber with an angle of approximately 55° with respect to the surface normal. Consequently, the desorption spots produced by the laser pulses on the crystal were elliptical. The desorption spot sizes measured using the spatial autocorrelation method (27) were approximately 490 μm in diameter along the major axis and 280 μm in diameter along the minor axis.

The use of LITD techniques for surface kinetic analysis has been described earlier (24,25,27-30). Briefly, the laser beam was translated on the Si(111) 7x7 surface using mirrors mounted on piezoelectric translation stages. For these LITD experiments, each new spatial location was interrogated with one laser pulse. A total of 250 different spots could be probed on the Si(111) 7x7 surface during one experiment. The spatial separation between adjacent positions

was approximately 520 μm along the major axes and 300 μm along the minor axes of the elliptical desorption areas.

Temperature-programmed LITD experiments were performed after Cl_2 exposures using a linear temperature ramp of $\beta = 2$ K/s. For the LITD and TPD experiments, the crystal was positioned approximately 5 cm in front of the ionizer of the quadrupole mass spectrometer. After saturation Cl_2 exposures, LITD signals were monitored for Cl, SiCl, $SiCl_2$ and $SiCl_3$ at m= 35, 63, 98 and 133 amu. These were the only LITD mass spectrometric signals observed between 1 -200 amu. No LITD signals were observed without electron impact ionization. The quadrupole mass spectrometer was controlled by a computer and alternated between the various masses. Consequently, all four masses were monitored simultaneously.

The chlorine coverages on Si(111) 7x7 were obtained by dosing Cl_2 through a glass multichannel capillary array that was attached to a variable leak valve. A tantalum foil with a 5 mm X 5 mm aperture was positioned immediately in front of the glass capillary array. This foil mask spatially restricted the Cl_2 flux and minimized the amount of Cl_2 that could adsorb on the edges of the sample mount.

Temperature programmed desorption (TPD) spectra were obtained using a linear heating rate of $\beta = 9$ K/s. At low chloride coverages, the species observed in the TPD spectra were Cl, SiCl and $SiCl_2$ at m = 35, 63, 98 amu, respectively. At higher chloride coverages, additional TPD signals were obtained at m = 133 and 168 amu corresponding to $SiCl_3$ and $SiCl_4$. Desorption of the Cl, SiCl and $SiCl_2$ species was observed only when the crystal was positioned with line-of-sight to the ionizer of the mass spectrometer.

The surface chloride coverage was assumed to be proportional to the area under the SiCl TPD spectrum at approximately 950 K. This high temperature SiCl TPD signal was denoted as the β_1-state. All chloride coverages were determined with respect to the β_1-state SiCl TPD area obtained after a saturation Cl_2 exposure on Si(111) 7x7 at 110 K. The chloride coverage corresponding to the saturated β_1-state SiCl TPD area was designated by Θ_s.

X-ray photoemission spectroscopy (XPS) studies of chlorine adsorption on Si(111) 7x7

have determined that chlorine atoms are found only in the on-top, monochloride configuration following saturation exposures and annealing to 673 K (7). Scanning tunneling microscope (STM) studies have reported that these on-top chlorine atoms passivate all the rest atoms in the 7x7 reconstruction (21). From these studies, the chloride coverage following saturation exposure and annealing to 673 K corresponds approximately to the total density of rest atoms, i.e. Θ_s = 6.7 X 10^{14} chlorine atoms/cm^2. Prior to annealing, the actual chloride coverage may be higher than the density of rest-atoms because di- and trichlorides can form after large Cl_2 exposures at low adsorption temperatures. The di- or trichlorides are removed, but the saturated β_1-state SiCl TPD area is not changed following annealing to 673 K (7,21).

The SiCl and $SiCl_2$ LITD signals were calibrated for all chloride coverages on Si(111) 7x7 using the SiCl TPD areas. These calibrations were performed by collecting SiCl and $SiCl_2$ LITD signals after a given Cl_2 exposure. The SiCl and $SiCl_2$ LITD signals were monitored at a variety of surface temperatures. The surface chloride coverage was then determined by measuring the β_1-state SiCl TPD area. These calibrations revealed a linear relationship between the SiCl and $SiCl_2$ LITD signals and the SiCl TPD areas at all chloride coverages.

III. Results

A. Temperature-Programmed Desorption

The TPD spectra obtained at chloride coverages of Θ/Θ_s = 0.39 and Θ/Θ_s= 1.00 are displayed in Figs. 1 and 2, respectively. The TPD spectra were obtained using a heating rate of β = 9 K/s following Cl_2 exposure at 110 K. Mass spectrometer signals for Cl, SiCl and $SiCl_2$ were observed at 950 K for both coverages. At Θ/Θ_s = 0.39, the TPD spectra in Fig. 1 are equivalent to the TPD spectra following $SiCl_4$ adsorption on Si(111) 7x7 (28). This earlier study assigned the SiCl and Cl desorption signals to the electron impact fragmentation of $SiCl_2$ (28).

At Θ/Θ_s = 1.0, additional Cl, SiCl and $SiCl_2$ desorption signals were observed at 690 K.

The low temperature SiCl TPD signal at 690 K was denoted as the β_2-state. As mentioned earlier, the high temperature SiCl TPD signal at 950 K was identified as the β_1-state. At $\Theta/\Theta_s = 1.00$, $SiCl_3$ and $SiCl_4$ desorption signals were also observed at 950 K. $SiCl_3$ is a major electron impact cracking fragment of $SiCl_4$ (31).

Figure 3a shows a series of SiCl TPD spectra versus chloride coverage. At lower chloride coverages of $\Theta/\Theta_s < 0.6$, only the β_1-state SiCl TPD signal is observed between 950 - 1000 K. These β_1-state SiCl TPD spectra are nearly equivalent to the SiCl TPD spectra following $SiCl_4$ exposures on Si(111) 7x7 (28) and $SiCl_4$-H_2 exposures on Si(111) 7x7 (32). At higher chloride coverages of $\Theta/\Theta_s > 0.6$, the β_2-state SiCl TPD signal is observed at 690 K.

Figure 3b shows a series of $SiCl_3$ TPD spectra versus chloride coverage. $SiCl_3$ desorption is only observed at higher chloride coverages of $\Theta/\Theta_s > 0.6$. The ratio of the TPD areas for $SiCl_3$: $SiCl_4$ is 1 : 0.65. This ratio is similar to the ratio of 1 : 0.4 measured by the mass spectrometer for the electron impact fragmentation of $SiCl_4$. Previous measurements of the electron impact fragmentation of $SiCl_4$ have reported a $SiCl_3$: $SiCl_4$ ratio of 1 : 0.6 (31). The ratio of the $SiCl_3$ and $SiCl_4$ TPD areas suggests that the $SiCl_3$ and $SiCl_4$ TPD signals are both derived from the desorption of $SiCl_4$.

The growth of the low temperature, β_2-state SiCl TPD signal as a function of surface chloride coverage is displayed in Fig. 4. As suggested by the SiCl TPD spectra in Fig. 3a, the low temperature β_2-state SiCl TPD signal appears at higher chloride coverages of $\Theta/\Theta_s > 0.6$. Figure 4 shows that the β_2-state SiCl TPD area grows progressively as a function of chloride coverage for coverages above $\Theta/\Theta_s = 0.6$.

B. Temperature-Programmed Laser Induced Thermal Desorption

The only species detected in the LITD yield following a saturation exposure of Cl_2 on Si(111) 7x7 were Cl, SiCl, $SiCl_2$ and $SiCl_3$. No Cl_2 or $SiCl_4$ LITD signals were observed. The temperature dependence of the Cl, SiCl and $SiCl_2$ LITD signals at m = 35, 63 and 98 amu for $\Theta/\Theta_s = 1.0$ is displayed in Fig. 5. For this temperature programmed LITD experiment, the silicon

sample was heated linearly at β = 2 K/s following a saturation Cl_2 exposure on Si(111) 7x7 at 110 K.

The decrease of the Cl, SiCl and $SiCl_2$ LITD signals between 900 - 1000 K is consistent with the thermal desorption of $SiCl_2$ (28). The Cl, SiCl and $SiCl_2$ LITD signals were scaled to determine if the LITD signals were all proportional to each other. This scaling revealed that the Cl, SiCl and the $SiCl_2$ LITD signals were superimposable after scaling. In correspondence with earlier studies of $SiCl_4$ on Si(111) 7x7 (28), these results indicate that the Cl, SiCl and $SiCl_2$ LITD signals originate from the electron impact fragmentation of $SiCl_2$. Consequently, the $SiCl_2$ LITD yield was probed by monitoring either the SiCl or $SiCl_2$ LITD signals.

The temperature dependence of the $SiCl_3$ LITD signal at m = 133 for Θ/Θ_S =1.0 following a saturation Cl_2 exposure at 110 K is shown in Fig. 6. The corresponding temperature dependence of the $SiCl_2$ LITD signal is also shown for comparison. Figure 6 reveals that the $SiCl_3$ LITD signal decreases between 650 - 750 K. Figures 5 and 6 also reveal that the Cl, SiCl, $SiCl_2$ and $SiCl_3$ LITD signals all increase gradually with surface temperature. This behavior is caused by the temperature dependence of the LITD signals and should not be confused with an actual increase in surface coverage (33,34).

C. LITD Product Yield versus Cl_2 Exposure

The growth of surface chloride species on the Si(111) 7x7 surface was studied as a function of Cl_2 exposure using LITD techniques. In these experiments, the clean Si(111) 7x7 surface was maintained at 110 K. Chlorine was then adsorbed on the Si(111) 7x7 surface by introducing Cl_2 through a second glass capillary array that was positioned directly above the electron impact ionizer of the mass spectrometer. The angle between the Cl_2 flux and the normal to the Si(111) 7x7 surface was approximately 45°.

During the adsorption of Cl_2 on the silicon surface, the chloride coverage was measured as a function of time by monitoring the $SiCl_2$ and $SiCl_3$ LITD signals. The laser beam was translated

along horizontal lines on the Si(111) 7x7 surface and a new surface position was interrogated for each LITD signal. By measuring the $SiCl_2$ and $SiCl_3$ LITD signals from different positions at different times during the Cl_2 exposure, the chloride coverage on Si(111) 7x7 was monitored in real time.

The $SiCl_2$ and $SiCl_3$ LITD signals are shown in Fig. 7. The $SiCl_2$ LITD signal was characterized by a rapid growth that was followed by saturation behavior at longer Cl_2 exposure times. In contrast, the $SiCl_3$ LITD signal was observed only after the $SiCl_2$ LITD signal had reached approximately 60% of the magnitude of the $SiCl_2$ LITD signal at saturation coverage. The $SiCl_3$ LITD signal was also characterized by a rapid, although delayed, growth followed by saturation behavior after longer Cl_2 exposures.

The SiCl and $SiCl_3$ LITD signals were examined as a function of surface temperature during Cl_2 exposure. In these experiments, the Si(111) 7x7 surface was exposed to a saturation Cl_2 exposure at different adsorption temperatures using the glass capillary array doser. LITD signals for SiCl ($SiCl_2$) and $SiCl_3$ at m = 63 and 133 amu were then measured at 400 K.

Figure 8 displays the LITD signals at 400 K for SiCl ($SiCl_2$) and $SiCl_3$ as a function of adsorption temperature. The SiCl ($SiCl_2$) and $SiCl_3$ LITD signals have been normalized to the SiCl ($SiCl_2$) and $SiCl_3$ LITD signals obtained at 120 K. Figure 8 shows that the SiCl ($SiCl_2$) LITD signals remain constant for adsorption temperatures between 120 K and 600 K. In contrast, the $SiCl_3$ LITD signals decrease dramatically from 120 K to 600 K.

D. Chlorine Surface Diffusion

Chlorine surface diffusion was measured on Si(111) 7x7 following Cl_2 exposures. Using LITD techniques (27,35), no chlorine surface diffusion was measurable. The experiments were performed using elliptical desorption holes with a 280 μm diameter along the minor axis and a 490 μm diameter along the major axis. These LITD prepare-and-probe investigations monitored no diffusional refilling signals at delay times as long as 2340 s for temperatures as high as 725 K.

The LITD surface diffusion studies place an upper limit on the chlorine surface diffusion coefficient. SiCl ($SiCl_2$) LITD signals at surface temperatures of 725 K can be measured easily for chlorine coverages of $\Theta \geq 0.05\ \Theta_s$ (28). Consequently, given that the chlorine coverage in the elliptical desorption hole is $\Theta \leq 0.05\ \Theta_s$ at delay times up to 2340 s, the chlorine surface diffusion coefficient must be $D \leq 5 \times 10^{-11}$ cm^2/s at 725 K.

IV. Discussion

A. TPD Product Yield

At low chloride coverages of $\Theta/\Theta_s < 0.6$, only Cl, SiCl and $SiCl_2$ mass spectrometric signals were observed in the TPD spectra. Similar TPD signals have also been observed in a previous study of $SiCl_4$ adsorption on Si(111) 7x7 (28). The ratio of the SiCl : $SiCl_2$ TPD areas was 2.4 : 1 at all chloride coverages following Cl_2 exposures. This ratio is similar to the SiCl : $SiCl_2$ TPD area ratio of 2.1 : 1 observed following $SiCl_4$ adsorption on Si(111) 7x7 (28). The Cl, SiCl and $SiCl_2$ TPD signals were all consistent with the electron impact fragmentation of $SiCl_2$ (28).

Isothermal desorption studies revealed that $SiCl_2$ desorption from Si(111) 7x7 following $SiCl_4$ adsorption displayed second-order desorption kinetics (28). Second-order desorption kinetics are consistent with a recombinative desorption mechanism involving $SiCl + Cl \rightarrow SiCl_2$. (28). In support of this mechanism, XPS studies have shown that monochloride species exist on the Si(111) 7x7 surface following $SiCl_4$ adsorption (8). The photoemission studies only observed Si(I) species after 100 and 1000 L exposures of $SiCl_4$ on the Si(111) 7x7 surface at 300 K (8). The Si(I) notation designates silicon surface atoms in an oxidation state of one that are bonded to one chlorine atom.

The TPD products are equivalent after exposures of $SiCl_4$ and Cl_2 that yield low chloride coverages of $\Theta/\Theta_s < 0.6$ on Si(111) 7x7. XPS studies have monitored the oxidation state of silicon surface atoms at 300 K as a function of chloride coverage on Si(111) 7x7 (8). At high chloride

coverage, Si(I), Si(II) and Si(III) species have been observed that are consistent with one, two and three chlorine atoms bonded to individual surface silicon atoms (7). However, only monochloride species are observed at low chloride coverage (8). STM studies of chlorine on Si(111) 7x7 surfaces have also shown that at low surface chloride coverages, chlorine reacts with the adatom dangling bonds to form SiCl species (22).

The similarity between the desorption products following $SiCl_4$ and Cl_2 adsorption on Si(111) 7x7 suggests that a recombinatory desorption mechanism involving $SiCl + Cl \rightarrow SiCl_2$ is applicable for $SiCl_2$ desorption following Cl_2 adsorption (28). A Redhead analysis (36) of the peak temperatures of the SiCl TPD spectra for various chloride coverages revealed a desorption activation barrier of E_d = 71 kcal/mole and a desorption preexponential of $\nu_d = 90\ cm^2/sec$. This analysis assumed second-order desorption kinetics and $\Theta_s = 6.7 \times 10^{14}$ chlorine atoms/cm^2 (21). These desorption kinetic parameters are in good agreement with E_d = 69 kcal/mole and $\nu_d = 4.1\ cm^2/sec$ derived from a similar Redhead analysis of the $SiCl_2$ TPD spectra and E_d = 67 kcal/mol and $\nu_d = 3.2\ cm^2/s$ obtained from isothermal measurements of $SiCl_2$ desorption following $SiCl_4$ exposure on Si(111) 7x7 (28).

At higher chloride coverages at $\Theta/\Theta_s > 0.6$, additional Cl, SiCl and $SiCl_2$ desorption features are observed in Figs. 2 and 3 at 695 K. The desorption of $SiCl_2$ from this low temperature, β_2-state is correlated with the disappearance of the $SiCl_3$ LITD signal. Figure 6 reveals that the $SiCl_3$ LITD signal decreases between approximately 500 and 800 K, whereas Fig. 1 shows that SiCl ($SiCl_2$) desorbs from the β_2-state between approximately 580 and 780 K. In addition, both the $SiCl_3$ LITD signal and β_2-state SiCl ($SiCl_2$) TPD signal appear at higher chloride coverages of $\Theta/\Theta_s > 0.6$. This correlation suggests that the $SiCl_3$ LITD signal and the β_2-state SiCl ($SiCl_2$) TPD signal originate from similar silicon-chloride surface species.

No $SiCl_3$ or $SiCl_4$ TPD signals were observed in Fig. 2 at the desorption temperature of 690 K corresponding to the β_2-state SiCl ($SiCl_2$) TPD signal. The ratio of the SiCl : $SiCl_2$ TPD areas for the β_2-state SiCl ($SiCl_2$) signal is 2.2 : 1. The similarity between this ratio and the SiCl :

$SiCl_2$ TPD area ratio of 2.4 : 1 obtained for the high-temperature β_1-state SiCl ($SiCl_2$) TPD signal indicates that the β_2-state SiCl ($SiCl_2$) TPD signal corresponds to additional $SiCl_2$ desorption.

B. LITD Product Yield

$SiCl_2$ is the only LITD product monitored following Cl_2 adsorption on Si(111) 7x7 at low chloride coverages of $\Theta/\Theta_s < 0.6$. $SiCl_2$ LITD products have also been detected following $SiCl_4$ adsorption on Si(111) 7x7 (28). In the $SiCl_4$ studies, $SiCl_2$ was the only desorption product observed at all surface chloride coverages by both TPD and LITD experiments (28). As mentioned earlier, the presence of the $SiCl_2$ LITD product can be explained by a recombinative desorption mechanism involving $\mathbf{SiCl + Cl \rightarrow SiCl_2}$ (28).

Figure 7 shows that $SiCl_3$ LITD species are observed at higher chloride coverages of $\Theta/\Theta_s > 0.6$ following larger Cl_2 exposures on Si(111) 7x7. These $SiCl_3$ LITD signals may be desorbed directly or may be derived from a recombinatory desorption mechanism involving $\mathbf{SiCl_2 + Cl \rightarrow SiCl_3}$. In addition, the $SiCl_3$ LITD signals may result from the cracking of $SiCl_4$ in the electron impact ionizer of the mass spectrometer. $SiCl_4$ may be produced by a recombinatory desorption mechanism involving $\mathbf{SiCl_3 + Cl \rightarrow SiCl_4}$.

If $SiCl_4$ is the primary desorption product, an $SiCl_4$ LITD signal at m = 168 amu corresponding to the $SiCl_4$ parent should be observed. However, no $SiCl_4$ LITD signal is observed at m = 168 amu. The measured relative intensities in the electron impact fragmentation pattern for $SiCl_4$ were 1 : 0.56 : 0.22 : 0.15 for SiCl : $SiCl_3$: $SiCl_4$: $SiCl_2$. These relative intensities contrast slightly with previous measurements of 1 : 0.6 : 0.31 : 0.078 for $SiCl_3$: $SiCl_4$: SiCl : $SiCl_2$ (31). However, the absence of $SiCl_4$ in the LITD mass spectrum indicates that the recombinatory desorption process involving $\mathbf{SiCl_3 + Cl \rightarrow SiCl_4}$ is negligible.

The direct desorption of $SiCl_3$ or the recombinatory desorption of $\mathbf{SiCl_2 + Cl}$ would argue that $SiCl_2$ and/or $SiCl_3$ species exist on the silicon surface. The presence of surface $SiCl_2$ and $SiCl_3$ species is consistent with XPS studies that have indicated that $SiCl_2$ and $SiCl_3$ are formed

as a function of increasing chloride coverage (8). In addition, $SiCl_2$ and $SiCl_3$ have been identified directly using STM by a measurement of the registry of the adatoms with respect to the underlying rest atom layer (22).

The appearance of the $SiCl_3$ LITD signal without a corresponding $SiCl_4$ LITD signal demonstrates that either $SiCl_3$ is desorbed directly or desorbed recombinatively via $SiCl_2 + Cl \rightarrow SiCl_3$. The ability of rapid laser induced heating to desorb silicon surface reaction intermediates has been demonstrated previously (37). For example, SiOH (29) and $SiNH_2$ (30) have been desorbed from Si(111) 7x7 surfaces exposed to H_2O and NH_3, respectively. For these silicon reaction intermediates, the correlation between the coverage of the SiOH and $SiNH_2$ species and the SiOH and $SiNH_2$ LITD signals has been established recently using transmission FTIR studies (38-40).

The $SiCl_3$ LITD signal and the β_2-state of the SiCl ($SiCl_2$) TPD spectrum appear at chloride coverages of $\Theta/\Theta_s > 0.6$ and grow progressively as a function of chloride coverage. This correspondence implies a common origin for these desorption products. However, $SiCl_3$ is the LITD product and $SiCl_2$ is the TPD product. These different desorption products suggest that the LITD heating rates of $\beta \approx 10^{10}$ K/sec and the TPD heating rates of $\beta \approx 10$ K/sec may access different desorption channels.

The ability of the heating rate to dictate kinetic pathways is the consequence of different kinetic channels with competing kinetic parameters (41,42). LITD can be employed as a kinetic probe of surface reaction intermediates because rapid laser-induced heating rates and large desorption preexponentials often select the desorption pathway instead of the reaction pathway (41,42). Consequently, the direct desorption of $SiCl_3$ or the recombinative desorption of $SiCl_2 + Cl \rightarrow SiCl_3$ may be favored at rapid laser-induced heating rates. In contrast, the same $SiCl_3$ or $SiCl_2$ species may thermally decompose and recombinatively desorb as $SiCl + Cl \rightarrow SiCl_2$ at slower heating rates.

C. Nature and Stability of Silicon-Chloride Species

1. Effect of Surface Temperature and Chloride Coverage

XPS studies of chlorine adsorption on Si(111) 7x7 have determined that mono-, di- and trichlorides are found on the silicon surface following a saturation exposure at 300 K (7,8). XPS studies have also demonstrated that only monohydride species remain after annealing a Si(111) 7x7 surface to 673 K following a saturation chlorine exposure (7). The presence of only monochloride species after annealing above 673 K has also been confirmed by UPS (9) and SEXAFS (13) studies.

Figure 6 shows that the $SiCl_3$ LITD signal has been reduced substantially by 700 K. The depletion of $SiCl_3$ LITD signals between 500 - 700 K is consistent with the XPS observation that the higher silicon-chloride species from the Si(111) 7x7 surface are removed at surface temperatures above 673 K (7). Only the $SiCl_2$ LITD signal is present above 700 K. The $SiCl_2$ LITD signal has been attributed to monochloride species and the recombinative desorption of SiCl + Cl $\rightarrow$ $SiCl_2$.

XPS studies have also shown that the presence of di- and trichloride species on the Si(111) 7x7 surface is dependent on the chloride coverage (8). Silicon di- and trichloride species were observed at high surface chloride coverages (8). In agreement with these XPS studies, Fig. 7 shows that $SiCl_3$ LITD signals are only observed after the $SiCl_2$ LITD signal has reached 60% of the $SiCl_2$ LITD signal magnitude at saturation coverage.

2. Effect of Adsorption Temperature

Figure 8 clearly shows that the $SiCl_3$ LITD signals following saturation Cl_2 exposures are strongly dependent on the adsorption temperature. The $SiCl_3$ LITD signals are the largest following saturation Cl_2 exposures at 120 K. The magnitude of the $SiCl_3$ LITD decreases progressively with increasing adsorption temperature. At 600 K, the $SiCl_3$ LITD signal following a saturation Cl_2 exposure is less than 5 times the $SiCl_3$ LITD signal observed at 120 K.

In contrast to the $SiCl_3$ LITD signal, the SiCl ($SiCl_2$) LITD signals are independent of

adsorption temperature. For adsorption temperatures between 120 - 600 K, the SiCl ($SiCl_2$) LITD signals are constant following saturation Cl_2 exposures. This constancy suggests that the saturated SiCl ($SiCl_2$) LITD signal represents a silicon surface where all the dangling bonds are tied up with monochloride species.

The temperature dependence of the SiCl ($SiCl_2$) and $SiCl_3$ LITD signals is analogous to the temperature dependence of the mono-, di- and trihydride species on Si(111) 7x7 following saturation hydrogen exposures. Infrared vibrational spectroscopy studies have revealed that the formation of monohydride species is independent of adsorption temperature (43). In addition, the β_1-state H_2 TPD areas obtained after saturation hydrogen exposures at various adsorption temperatures on Si(111) 7x7 were constant (44). Transmission FTIR studies on porous silicon have demonstrated that the β_1-state of the H_2 TPD spectrum corresponds with H_2 desorption from monohydride species (45).

Several previous studies have observed that the formation of di- and trihydride species on Si(111) 7x7 decreases with adsorption temperature (43,46,47). The magnitude of the SiH_3 (SiH_4) LITD signal from Si(111) 7x7 following a saturation hydrogen exposure also decreased with increasing adsorption temperature (44). The SiH_3 (SiH_4) LITD signal is associated with the β_2-state of the H_2 TPD spectrum from Si(111) 7x7 (44). Infrared studies have shown that the β_2-state of the H_2 TPD spectra corresponds with H_2 desorption from di- and trihydride species (45).

There are many similarities between the chlorides and hydrides on Si(111) 7x7. The monochlorides and monohydrides both saturate and reach a saturation coverage that is independent of adsorption temperature. In contrast, the stability of the di- and trichlorides and di- and trihydrides on Si(111) 7x7 are both very dependent on the coverage and the adsorption temperature between 120 - 600 K. Although the adsorption temperature is critical, the desorption or decomposition of both the di- or trichlorides and the di- or trihydride species do not occur until higher temperatures of 650 - 700 K (45,46).

D. Comparison with Previous Results

1. Temperature Programmed Desorption

A very early TPD study of a saturated chlorine coverage on a Si(111) 7x7 surface yielded Cl and $SiCl_x$ species where x = 1,2,3,4 (18). This study was performed at a heating rate of $\beta \approx 60$ K/s and a variety of desorption species were reported to desorb at 1143 K. The silicon-chloride species were assigned to the cracking of $SiCl_4$ in the ionizer of the mass spectrometer (18). However, a careful study of the relative abundance of each $SiCl_x$ species was not performed and the cracking pattern of $SiCl_4$ was not examined (18). Consequently, $SiCl_2$ and $SiCl_4$ may have both desorbed from the Si(111) surface with a saturated chlorine coverage and contributed to this early TPD spectrum.

Compared with the desorption yield from Si(111) 7x7, the desorption products and desorption temperatures following Cl_2 exposures on a Si(100) surface were quite different (20). In the recent studies on Si(100), two desorption states were obtained (20). A mixture of $SiCl_4$ and $SiCl_2$ desorbed from the β-state at 900 K (20). In contrast, $SiCl_4$ desorbed from the low-temperature, α-state at 450 K. This low temperature, α-state at 450 K did not saturate following large Cl_2 exposures and Cl_2 was reported to be adsorbed without limit.

The differences between the desorption yields following Cl_2 adsorption on Si(111) 7x7 and Si(100) may be related to the different structures of these surfaces. The Si(111) 7x7 surface has adatoms and a distinctive reconstruction described by the dimer-adatom-stacking fault model (48). In contrast, the Si(100) surface generally displays a 2x1 reconstruction and prominent silicon dimer pairs.

2. STM studies of chlorine on Si(111) 7x7

STM studies of chlorine on Si(111) 7x7 have been performed over the same temperature range as this experiment. These STM studies provide an interesting comparison with these LITD and TPD studies. For example, Fig. 6 shows the disappearance of the $SiCl_3$ LITD signal at

approximately 700 K. STM studies have shown that annealing a Si(111) 7x7 surface with a saturated chlorine coverage to 743 K produces an extensive structural rearrangement in which the adatoms have been stripped away and have accumulated in pyramidal silicon islands (23). The removal of the adatoms allows the rest atom layer to be imaged by the STM (21). Much of this rest atom layer exists as adatom-free domains that are stabilized with monochloride species (21-23).

The STM results for the various silicon-chloride species are also analogous to previous results for the temperature dependence of di- and trihydrides on Si(111) 7x7 (43,46,47). At low temperatures and high hydrogen coverages, STM studies have observed isolated adatoms and adatom islands on the Si(111) 7x7 surface (49). The isolated adatoms are believed to be either di- or trihydride species. The adatom islands are similar to the pyramidal silicon islands formed on the Si(111) 7x7 surface after annealing at 743 K following saturation chlorine exposures (23).

The STM studies of hydrogen on Si(111) 7x7 have observed that the isolated adatoms diffuse together to form adatom islands at higher hydrogen coverages and higher hydrogen exposure temperatures. The formation of adatom islands reduces the population of isolated adatoms (49). There are lower coverages of di- and trihydride species because monohydride species are believed to dominate on the adatom islands (49). Adatom islanding at higher chlorine coverages and higher chlorine exposure temperatures is also observed for chlorine on Si(111) 7x7 (23). The formation of these adatom islands from isolated adatoms may inhibit the formation of the higher chlorides at higher adsorption temperatures.

The formation of $SiCl_2$ and $SiCl_3$ on Si(111) 7x7 may be analogous to the formation of SiH_2 and SiH_3 because the higher chlorides and hydrides involve silicon adatoms (22,23,49). The desorption or decomposition of the higher chloride and hydride species may also be rate-limited by similar processes. The β_2-state of the H_2 TPD spectrum corresponding to H_2 desorption from di- and trihydrides occurs at approximately 700 K (45). Likewise, the β_2-state of the SiCl ($SiCl_2$) TPD spectrum and the loss of $SiCl_3$ LITD signals also occur at approximately 700 K. This correspondence suggests that the diffusion of isolated adatoms to form adatom islands may be rate-limiting the desorption or decomposition of the higher chlorides and hydrides on Si(111) 7x7

(50).

The intriguing correlation between the disappearance of the $SiCl_3$ LITD signal and the β_2-state of the SiCl ($SiCl_2$) TPD spectrum may also be rationalized based upon the diffusion of isolated adatoms to form adatom islands. There may be sufficient time for the isolated adatoms of $SiCl_3$ to diffuse and form adatom islands during slow TPD heating rates of $\beta \approx 10$ K/sec. Subsequently, the adatom islands may lead to the desorption of $SiCl_2$. In contrast, the direct desorption of the isolated adatoms of $SiCl_3$ may be favored during rapid LITD heating rates of $\beta \approx 10^{10}$ K/sec.

V. Conclusions

Desorption product yields obtained following Cl_2 adsorption on Si(111) 7x7 were studied using temperature-programmed desorption (TPD) and laser-induced thermal desorption (LITD) techniques. At low chloride coverages of $\Theta/\Theta_s < 0.6$, TPD experiments monitored $SiCl_2$ as the only desorption product at approximately 950 K. At higher chloride coverages of $\Theta/\Theta_s > 0.6$, a small $SiCl_4$ TPD signal was also monitored at 950 K along with an additional $SiCl_2$ TPD feature at 690 K.

LITD experiments detected $SiCl_2$ as the only desorption product in the LITD yield at low chloride coverages of $\Theta/\Theta_s < 0.6$. $SiCl_2$ and $SiCl_3$ LITD signals were both observed at higher chloride coverages of $\Theta/\Theta_s > 0.6$. The $SiCl_2$ desorption products were assigned to the recombinative desorption of $\mathbf{SiCl + Cl \rightarrow SiCl_2}$. Because the $SiCl_3$ LITD signals were not accompanied by $SiCl_4$ parent LITD signals, the $SiCl_3$ LITD signals were attributed to the direct desorption of $SiCl_3$ species or the recombinative desorption of $\mathbf{SiCl_2 + Cl \rightarrow SiCl_3}$.

In temperature-programmed LITD studies, the $SiCl_2$ LITD signals persisted until 950 K, whereas the $SiCl_3$ LITD signals were only observed until 700 K. In addition, the magnitude of the $SiCl_3$ LITD yield following saturation Cl_2 exposures decreased as a function of adsorption temperature. Based on photoemission and scanning tunneling microscopy investigations, the $SiCl_2$

and $SiCl_3$ desorption yields were correlated with the existence of mono-, di- and trichlorides on Si(111) 7x7. Many similarities were also observed between the chlorides and hydrides on the Si(111) 7x7 surface.

VI. Acknowledgements

This work was supported by the Office of Naval Research under Contract N00014-90-J-1281. Some of the equipment utilized in this work was provided by the NSF-MRL program through the Center for Materials Research at Stanford University. We acknowledge useful and stimulating conversations with Dr. John J. Boland. BGK also gratefully acknowledges the National Science Foundation for a graduate fellowship. SMG acknowledges the National Science Foundation for a Presidential Young Investigator Award and the A.P. Sloan Foundation for a Sloan Research Fellowship.

References

1. C.J. Mogab and H.J. Levinstein, J. Vac. Sci. Technol., **17** (1980) 721.
2. N.A. Takasaki, E.Ikawa and Y. Kurogi, J. Vac. Sci. Technol., **B4** (1986) 806.
3. S.C. McNevin and G.E. Becker, J. Vac. Sci. Technol., **B3** (1985) 485.
4. V.S. Ban and S.L. Gilbert, J. Electrochem. Soc., **122** (1975) 1382.
5. V.S. Ban, J. Electrochem. Soc., **122** (1975) 1389.
6. W.A.P. Claassen and J. Bloem, J. Cryst. Growth, **50** (1980) 807.
7. R.D. Schnell, D. Rieger, A. Bogen, F.J. Himpsel, K. Wandelt and W. Steinmann, Phys. Rev. **B32** (1985) 8057 .
8. L.J. Whitman, S.A. Joyce, J.A. Yarmoff, F.R. McFeely and L.J. Terminello, Surface Sci., **232** (1990) 297.
9. K.C. Pandey, T. Sakurai and H.D. Hagstrum, Phys. Rev. **B16** (1977) 3648.
10. P.K. Larsen, N.V. Smith, M. Schluter, H.H. Farrell, K.M. Ho and M.L. Cohen, Phys. Rev. **B17** (1978) 2612.
11. K. Mednick and C.C. Lin, Phys. Rev. **B17** (1978) 4807.
12. M. Schluter, J.E. Rowe, G. Margaritondo, K.M. Ho and M.L. Cohen, Phys. Rev. Letters **37** (1976) 1632.
13. P.H. Citrin, J.E. Rowe and P. Eisenberger, Phys. Rev. **B28** (1983) 2299.
14. G.B. Bachelet and M. Schluter, Phys. Rev. **B28** (1983) 2302.
15. M. Seel and P.S. Bagus, Phys. Rev. **B28** (1983) 2023.
16. G. Thornton, P.L. Wincott, R. McGrath, I.T. McGovern, F.M. Quinn, D. Norman and D.D. Vvedensky, Surface Sci., **211/212** (1989) 959.
17. N. Aoto, E. Ikawa and Y. Kurogi, Surface Sci., **199** (1988) 408.
18. J.V. Florio and W.D. Robertson, Surface Sci., **18** (1969) 398.
19. R.J. Madix and J.A. Schwarz, Surface Sci., **24** (1971) 264.
20. R.B. Jackman, H. Ebert and J.S. Foord, Surface Sci., **176** (1986) 183.

21. J.S Villarrubia and J.J. Boland, Phys. Rev. Letters, **63** (1989) 306.

22. J.J. Boland and J.S. Villarrubia, Science, **248** (1990) 838.

23. J.J. Boland and J.S. Villarrubia, Phys. Rev. **B41** (1990) 9865.

24. P. Gupta, C.H. Mak, P.A. Coon and S.M. George, Phys. Rev. **B40** (1989) 7739.

25. B.G. Koehler, C.H. Mak, D.A. Arthur, P.A. Coon and S.M. George, J. Chem. Phys., **89** (1988) 1709.

26. S.M. George, J. Vac. Sci. Technol., **A4** (1986) 2394.

27. S.M. George, A.M. DeSantolo and R.B. Hall, Surface Sci., **159** (1985) L425.

28. P. Gupta, P.A. Coon, B. G. Koehler and S.M. George, J. Chem. Phys., **93** (1990) 2827.

29. B.G. Koehler, C.H. Mak, and S.M. George, Surface Sci. **221** (1989) 565.

30. B.G. Koehler, P.A. Coon and S.M. George, J. Vac. Sci. Technol. B7 (1989) 1303.

31. H. J. Svec and G. R. Sparrow, J. Chem. Soc. (A), (1970) 1162.

32. P. Gupta, P.A. Coon, M.L. Wise and S.M. George, (*submitted to Surface Sci.*)

33. J.L. Brand and S.M. George, Surface Sci. **167** (1986) 341.

34. B.G. Koehler and S.M. George, (*Surface Sci., in press*)

35. C.H. Mak, J.L. Brand, A.A. Deckert and S.M. George, J. Chem. Phys., **85** (1986) 1676.

36 P.A. Redhead, Vacuum, **12** (1962) 203.

37. C.H. Mak, B.G. Koehler and S.M. George, Surface Sci. Letters, **208** (1989) L42.

38 P. Gupta, A.C. Dillon, P.A. Coon and S.M. George, (*Chem. Phys. Lett., in press*)

39. P. Gupta, A.C. Dillon, A.S. Bracker and S.M. George, (*Surface Sci., in press*)

40. A.C. Dillon, P. Gupta, M.B. Robinson, A.S. Bracker and S.M. George, (*submitted to J. Vac. Sci. Technol.*)

41. A.A. Deckert and S.M. George, Surface Sci. **182** (1987) L215.

42. R.B. Hall, J. Phys. Chem. **91** (1987) 1007.

43. U. Jansson and K.J. Uram, J. Chem. Phys., **91** (1989) 7978.

44. P.A. Coon, P. Gupta, B.G. Koehler and S.M. George, (*in preparation*).

45. P. Gupta, V.L. Colvin and S.M. George, Phys. Rev. **B37** (1988) 8234.

46. C.M. Greenlief, S.M. Gates and P.A. Holbert, J. Vac. Sci. Technol., A7 (1989) 1845.

47. H. Wagner, R. Butz, U. Backes and D. Bruchmann, Sol. State. Comm., **38** (1981) 1155.

48. K. Takayanagi, Y. Tanishiro, S. Takahashi and M. Takahashi, Surface Sci. **164** (1985) 367.

49. J.J. Boland, (*submitted to Surface Sci.*)

50. J.J. Boland, *private communication.*

Figure Captions

Figure 1. TPD mass spectra at β = 9 K/s for SiCl, $SiCl_2$, Cl, $SiCl_3$ and $SiCl_4$ from a chloride coverage of Θ/Θ_s = 0.39 on Si(111) 7x7.

Figure 2. TPD mass spectra at β = 9 K/s for SiCl, $SiCl_2$, Cl, $SiCl_3$ and $SiCl_4$ from a chloride coverage of Θ/Θ_s = 1.00 on Si(111) 7x7.

Figure 3. TPD mass spectra at β = 9 K/s for a) SiCl and b) $SiCl_3$ as a function of chloride coverage on Si(111) 7x7.

Figure 4. Normalized TPD signal of the β_2-state $SiCl_2$ TPD spectra as a function of chloride coverage on Si(111) 7x7.

Figure 5. LITD signals for SiCl, $SiCl_2$ and Cl versus surface temperature for a chloride coverage of Θ/Θ_s = 1.00 on Si(111) 7x7. The linear temperature ramp was β = 2 K/s.

Figure 6. LITD signals for $SiCl_2$ and $SiCl_3$ versus surface temperature for a chloride coverage of Θ/Θ_s = 1.00 on Si(111) 7x7. The $SiCl_3$ LITD signal has been multiplied by a factor of 12. The linear temperature ramp was β = 2 K/s.

Figure 7. LITD signals for $SiCl_2$ and $SiCl_3$ versus time during Cl_2 exposure on Si(111) 7x7 at 110 K. The $SiCl_3$ LITD signal has been multiplied by a factor of 10.

Figure 8. Normalized LITD signals for SiCl and $SiCl_3$ after saturation Cl_2 exposures on Si(111) 7x7 at various adsorption temperatures.

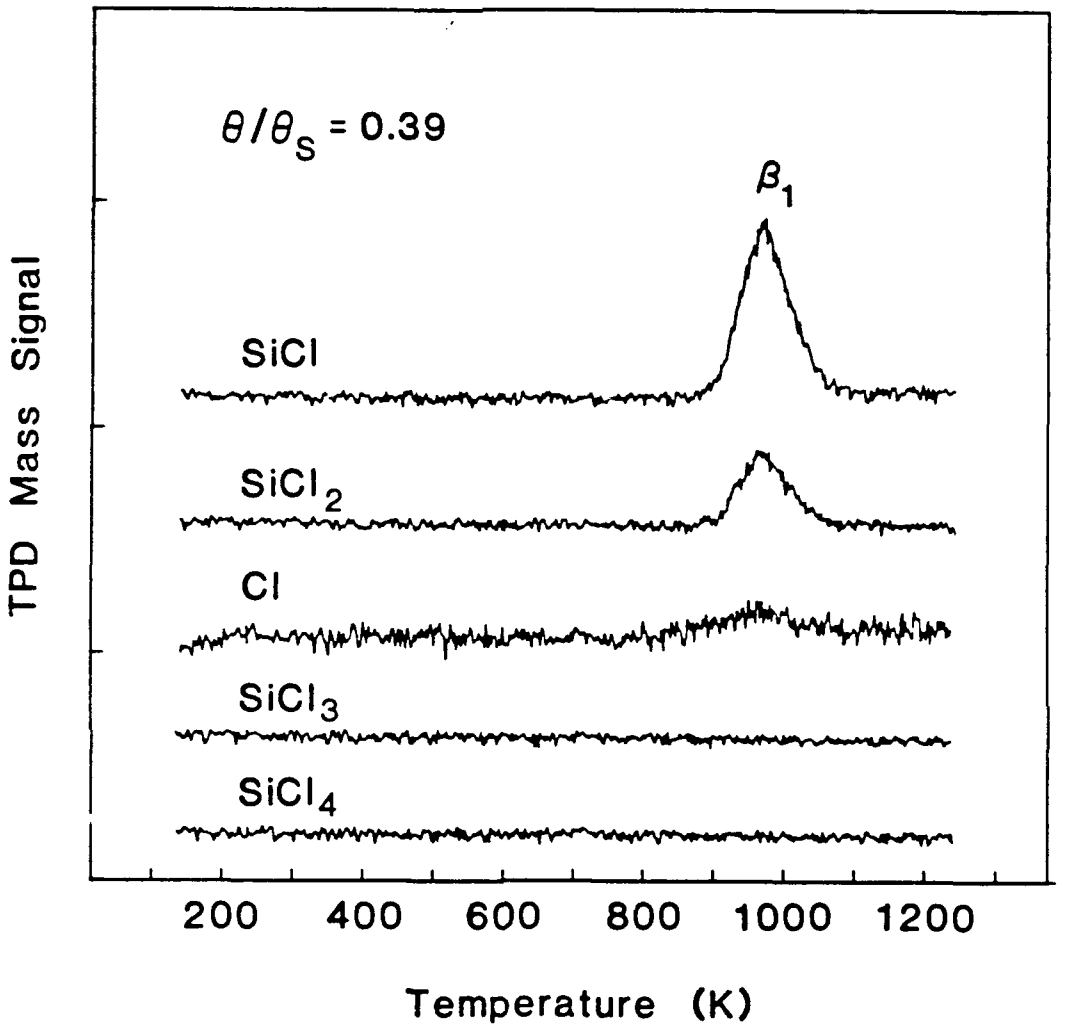
θ/θS = 0.39
β1
SiCl
SiCl2
Cl
SiCl3
SiCl4
TPD Mass Signal
200
400
600
800
1000
1200
Temperature (K)

Fig. 1

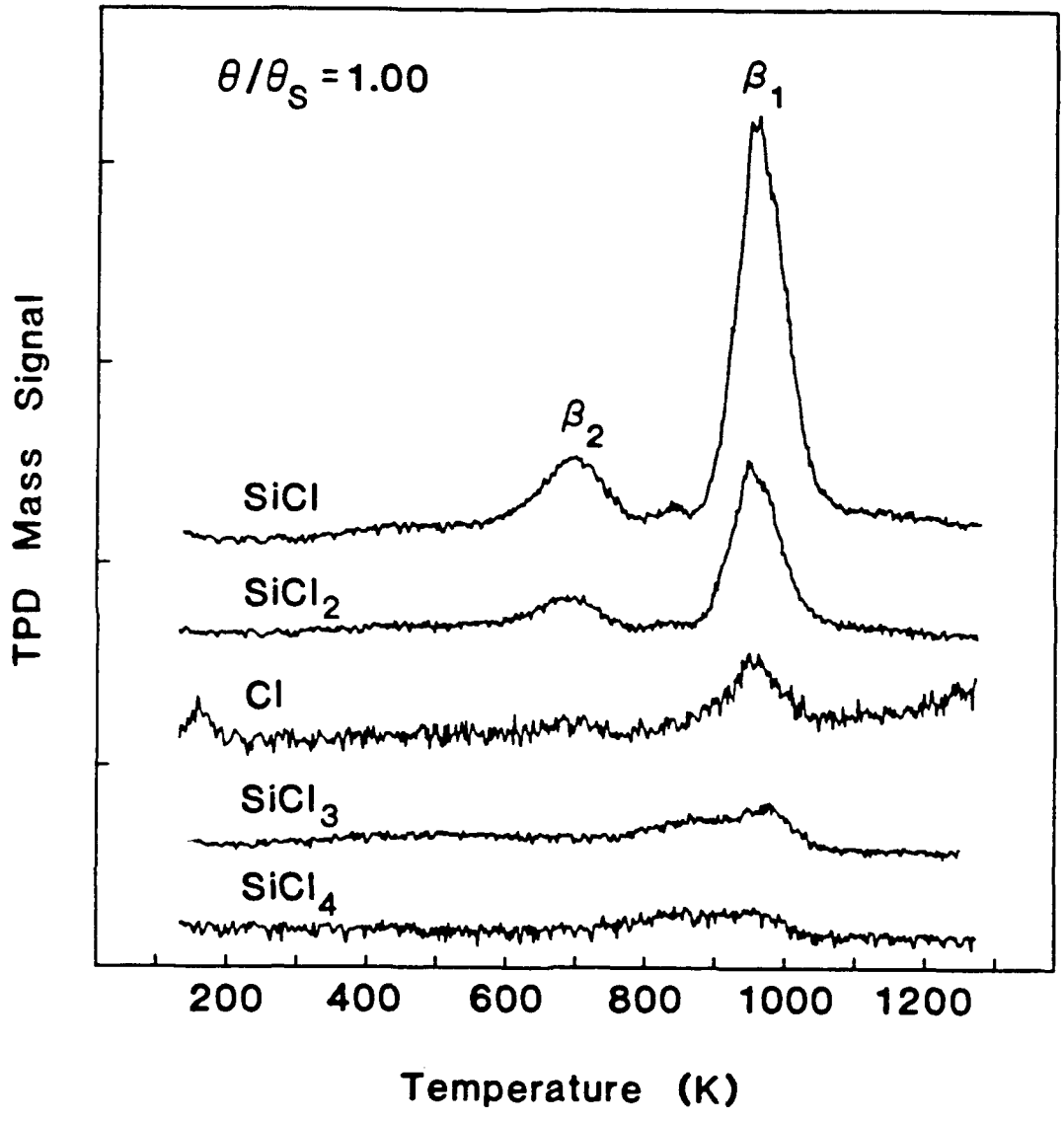
θ/θS = 1.00
β1
β2
SiCl
SiCl2
Cl
SiCl3
SiCl4
TPD Mass Signal
200
400
600
800
1000
1200
Temperature (K)

Fig. 2

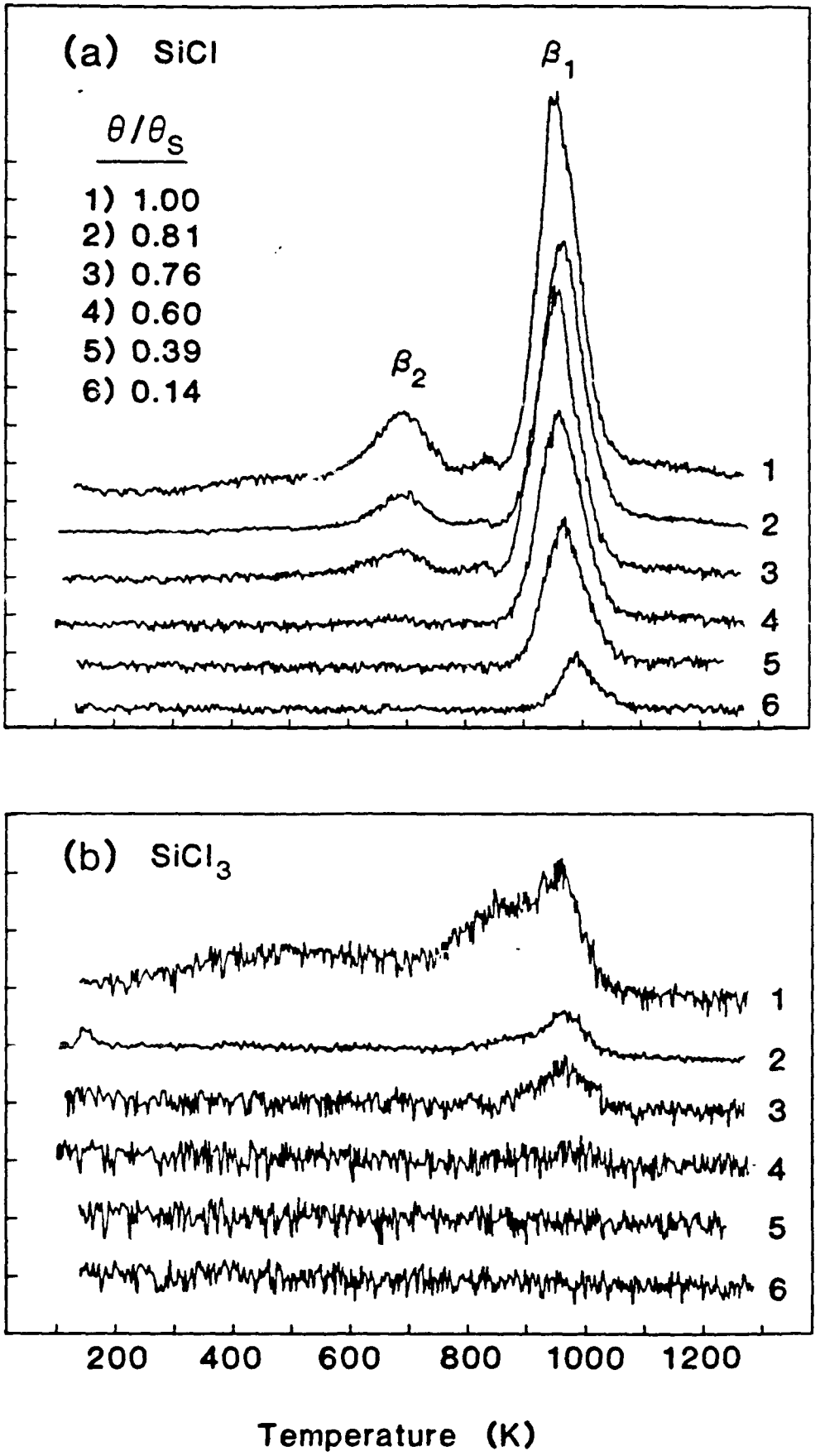
(a) SiCl
β_1
β_2
θ/θ_S
1) 1.00
2) 0.81
3) 0.76
4) 0.60
5) 0.39
6) 0.14
1
2
3
4
5
6
(b) $SiCl_3$
1
2
3
4
5
6
200
400
600
800
1000
1200
TPD Mass Signal
Temperature (K)

Fig. 3

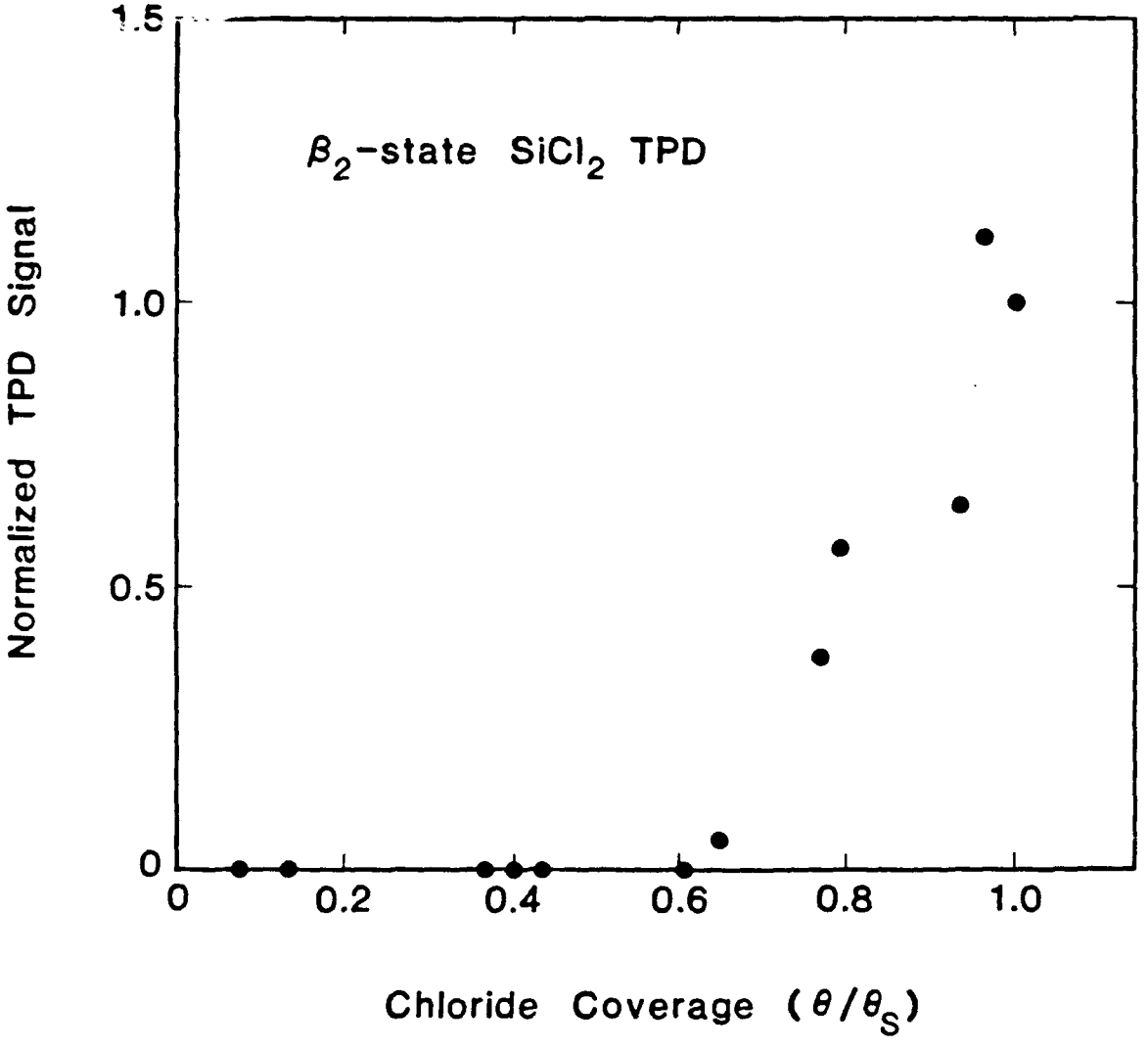
β_2-state $SiCl_2$ TPD
Normalized TPD Signal
1.5
1.0
0.5
0
0
0.2
0.4
0.6
0.8
1.0
Chloride Coverage (θ/θ_S)

Fig. 4

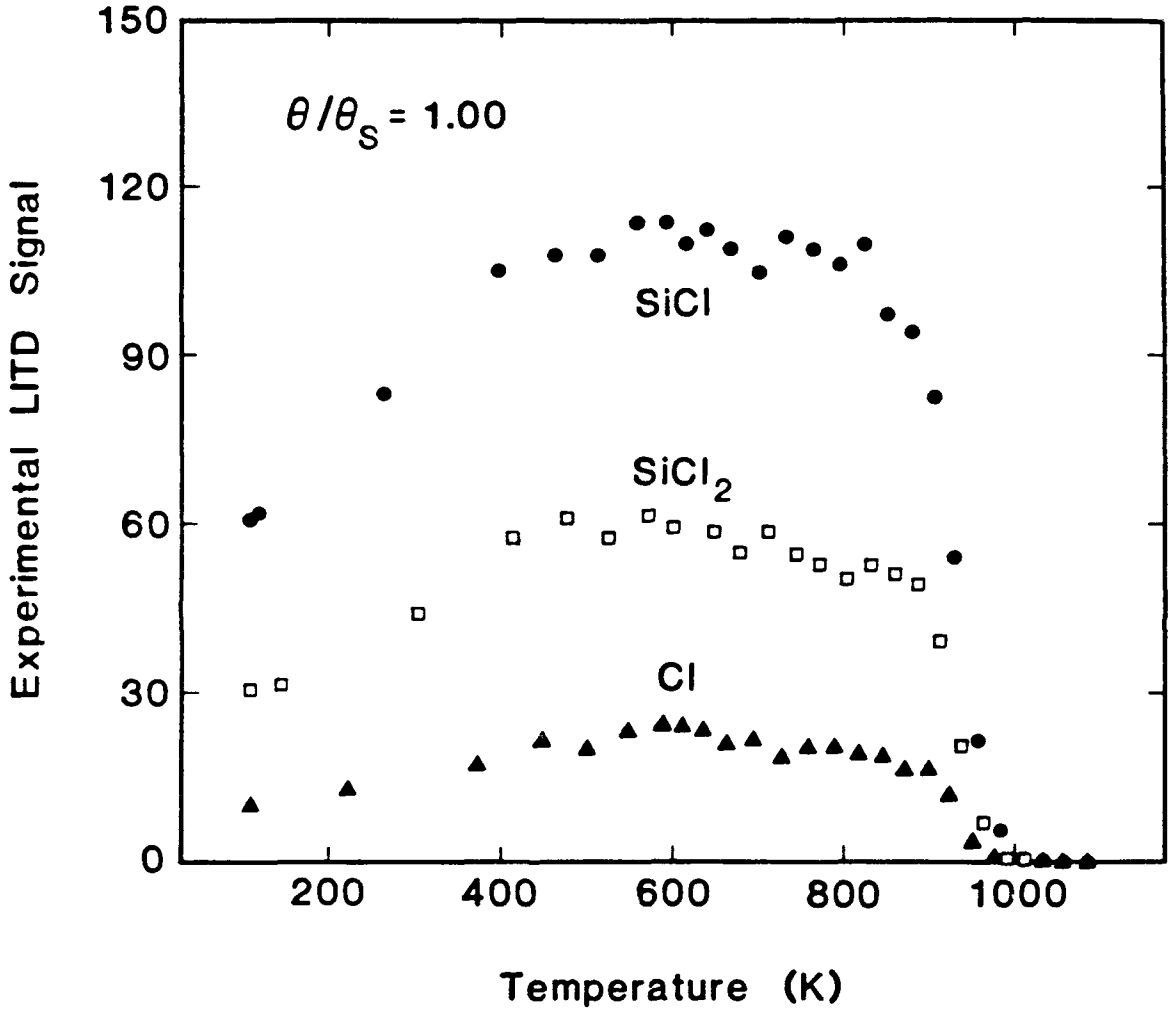
150
120
90
60
30
0
θ/θ_S = 1.00
SiCl
$SiCl_2$
Cl
200
400
600
800
1000
Experimental LITD Signal
Temperature (K)

Fig. 5

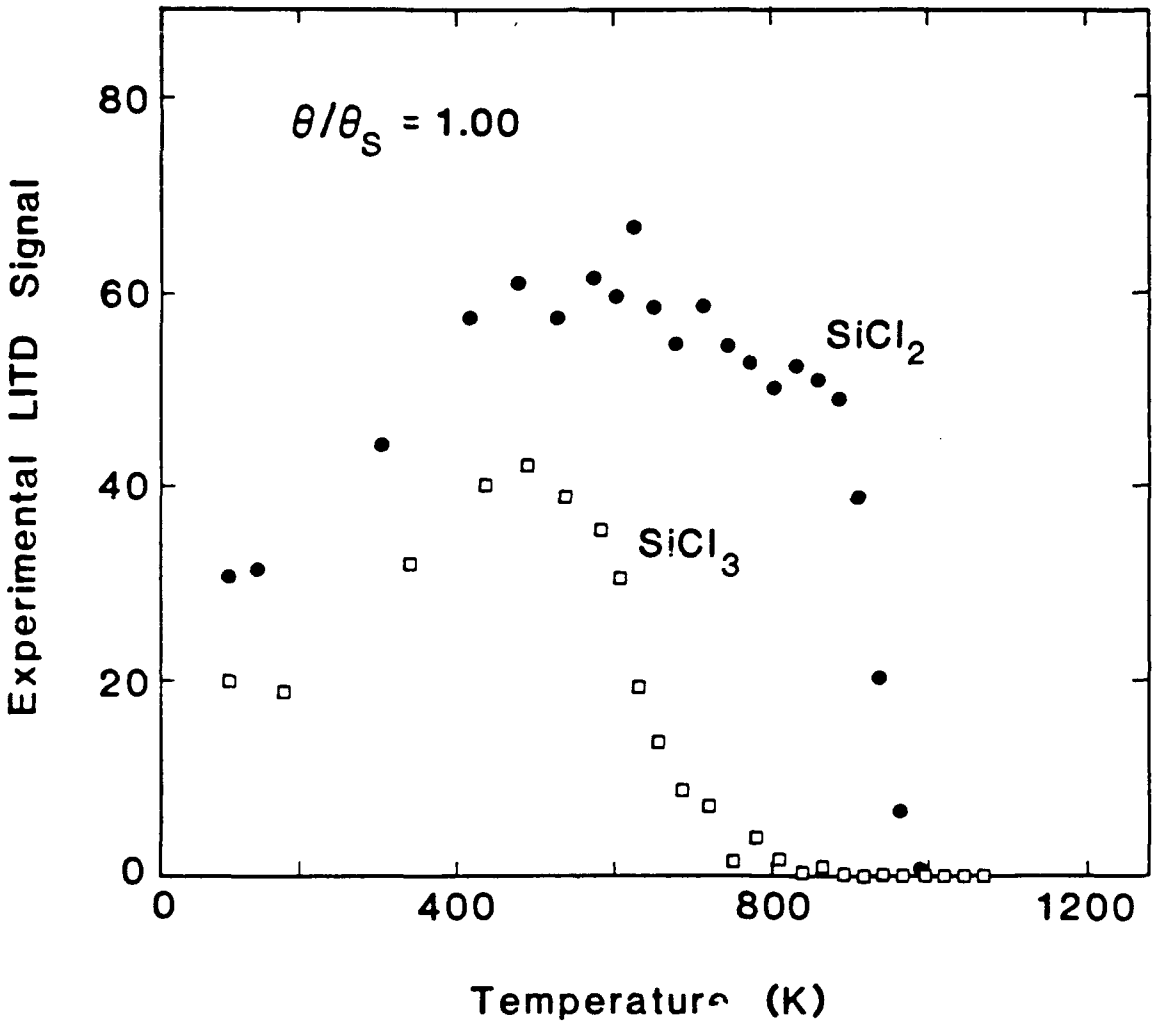
θ/θ_S = 1.00
$SiCl_2$
$SiCl_3$
Experimental LITD Signal
Temperature (K)
0
20
40
60
80
0
400
800
1200

Fig. 6

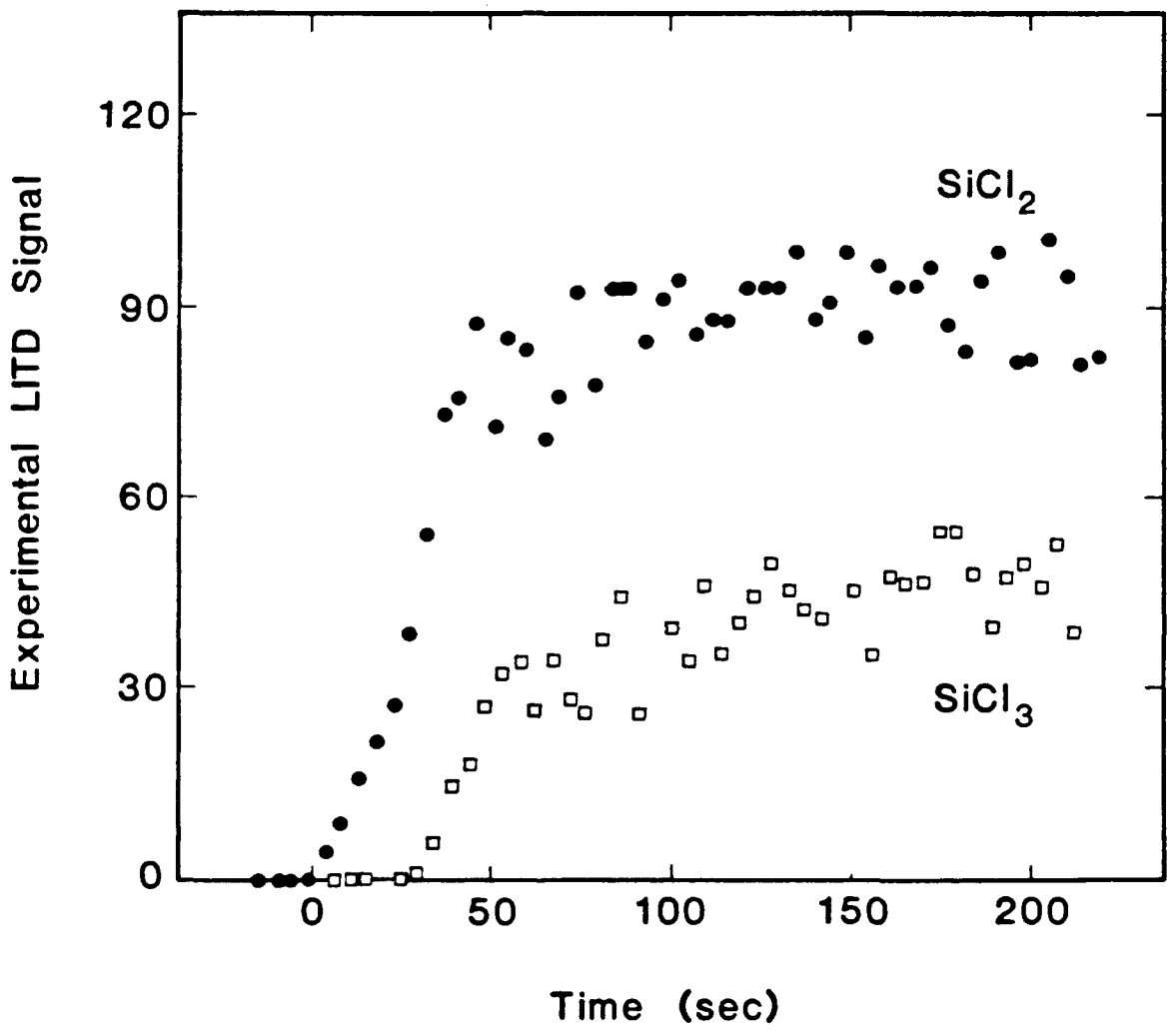
Experimental LITD Signal
120
90
60
30
0
0
50
100
150
200
Time (sec)
SiCl2
SiCl3

Fig. 7

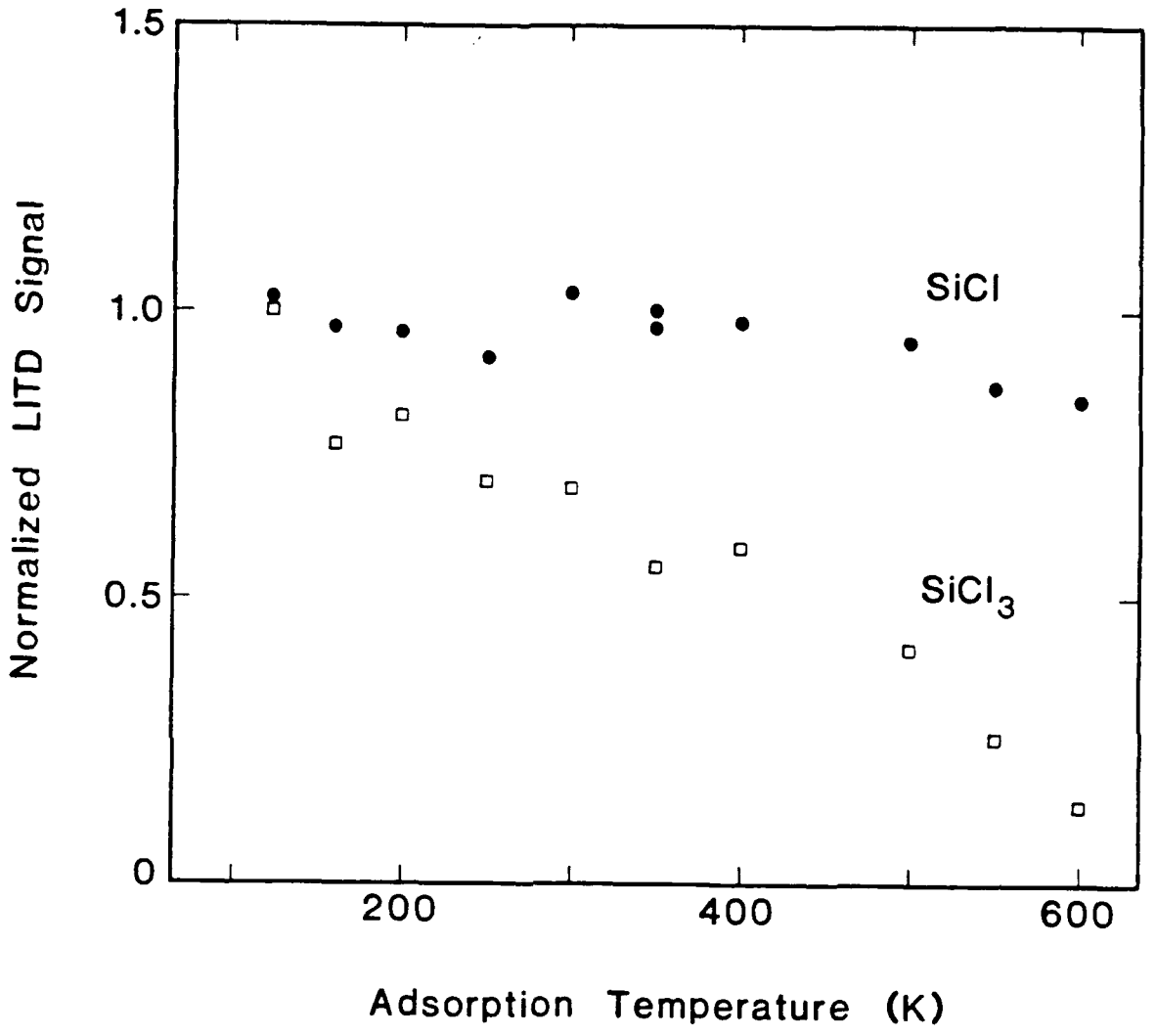
1.5
1.0
0.5
0
Normalized LITD Signal
SiCl
SiCl3
200
400
600
Adsorption Temperature (K)

Fig. 8